INTERNATIONAL JOURNAL FOR NUMERICAL METHODS IN FLUIDS
Int. J. Numer. Meth. Fluids **31**: 79–95 (1999)

A DISCONTINUOUS *hp* FINITE ELEMENT METHOD FOR THE EULER AND NAVIER–STOKES EQUATIONS

CARLOS ERIK BAUMANN[1] AND J. TINSLEY ODEN*,[2]

Texas Institute for Computational and Applied Mathematics, The University of Texas at Austin, Austin, TX 78712, USA

SUMMARY

This paper introduces a new method for the solution of the Euler and Navier–Stokes equations, which is based on the application of a recently developed discontinuous Galerkin technique to obtain a compact, higher-order accurate and stable solver. The method involves a weak imposition of continuity conditions on the state variables and on inviscid and diffusive fluxes across inter-element and domain boundaries. Within each element the field variables are approximated using polynomial expansions with local support; therefore, this method is particularly amenable to adaptive refinements and polynomial enrichment. Moreover, the order of spectral approximation on each element can be adaptively controlled according to the regularity of the solution. The particular formulation on which the method is based makes possible a consistent implementation of boundary conditions, and the approximate solutions are locally (elementwise) conservative. The results of numerical experiments for representative benchmarks suggest that the method is robust, capable of delivering high rates of convergence, and well suited to be implemented in parallel computers. Copyright © 1999 John Wiley & Sons, Ltd.

KEY WORDS: discontinuous Galerkin; Euler; Navier–Stokes

1. INTRODUCTION

A new discontinuous Galerkin technique is presented for the solution of the Euler and Navier–Stokes equations that supports an extended set of basis functions, including piecewise discontinuous approximations. The formulation is locally or elementwise conservative, it *does not require auxiliary variables* as do mixed or hybrid methods, and produces a mass matrix that is block diagonal (uncoupled blocks) for any degree of the polynomial basis functions.

The current trend in computational fluid dynamics (CFD) is to obtain high accuracy using reconstruction techniques [1–3] or large stencils, which are strongly dependent on the quality of the underlying mesh [4,5]. The approach in this paper is to attain higher accuracy using polynomial expansions within each element; this approach was introduced in References [6–9] for scalar problems, where *a priori* error estimates and stability analysis are presented.

Contrasting with other techniques that use discontinuous basis functions to discretize second-order diffusion operators and that lead to indefinite discrete approximations [10,11], the present formulation produces *positive definite* discrete approximations to the diffusive

* Correspondence to: Texas Institute for Computational and Applied Mathematics, The University of Texas at Austin, Austin, TX 78712, USA.
[1] Research Engineer, COMCO Inc., Austin, TX, USA.
[2] Director of TICAM, Cockrell Family Regents Chair in Engineering # 2.

CCC 0271–2091/99/170079–20$17.50

terms of the governing equations, which is fundamental for time-marching algorithms and for many iterative techniques.

The novelty of the method presented here is that it is a truly discontinuous Galerkin technique that handles the diffusion operators without resorting to a mixed formulation. This is very advantageous considering that for a problem in $\mathbb{R}^d$, using a mixed formulation, the number of state variables increases from $(d+2)$ to (d^2+2d+2) when the energy equation is included, and from $(d+1)$ to (d^2+d+1) when it is not included. Most of the discontinuous Galerkin solutions to the Navier–Stokes equations have been obtained using mixed formulations; see, for example, Bassi and Rebay [12,13], Lomtev *et al.* [14–17], Warburton *et al.* [18], and Cockburn and Shu in the development of the local discontinuous Galerkin method [19].

This paper is structured as follows. Section 2 introduces a model scalar convection–diffusion problem with the associated notation, and in Section 3 the associated discontinuous Galerkin approximation with *a priori* error estimation is presented. Then, notations for Euler and Navier–Stokes problems are introduced in Section 4, and the space discretizations with broken spaces in an infinite-dimensional setting are introduced in Section 5. The approximation with polynomial basis is described in Section 6. Finally, a number of numerical experiments are discussed in Section 7 and major conclusions of the study are collected in Section 8.

2. SCALAR CONVECTION–DIFFUSION PROBLEM

Let Ω be an open bounded Lipschitz domain in $\mathbb{R}^d$, such as the polygonal domain in $\mathbb{R}^2$ depicted in Figure 1. Consider a model second-order convection diffusion problem characterized by the following scalar partial differential equation and boundary conditions

$$-\nabla\cdot(\boldsymbol{A}\nabla u)+\nabla\cdot(\boldsymbol{\beta}u)+\sigma u=S, \quad \text{in } \Omega\subset\mathbb{R}^d \tag{1}$$

$$\begin{aligned} u &= f && \text{on } \Gamma_{\mathrm{D}} \\ (\boldsymbol{A}\nabla u)\cdot\boldsymbol{n} &= g && \text{on } \Gamma_{\mathrm{N}} \end{aligned} \tag{2}$$

where $\boldsymbol{\beta}\in(L^\infty(\Omega))^d$ is the mass flux vector, $\sigma\in L^\infty(\Omega)$, $\sigma>0$ a.e. in Ω, $S\in L^2(\Omega)$, and $\boldsymbol{A}\in(L^\infty(\Omega))^{d\times d}$ is a diffusivity matrix characterized as follows:

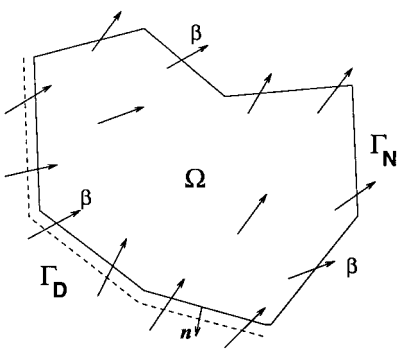

Figure 1. Domain and boundaries—notation.

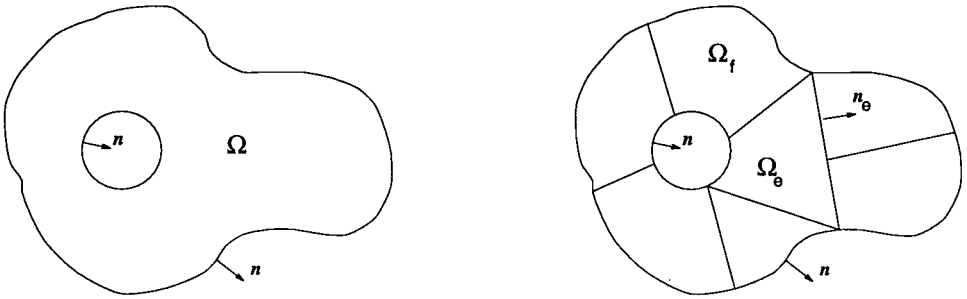

Figure 2. Domain and boundary—notation.

$$\boldsymbol{A}(\boldsymbol{x}) = \boldsymbol{A}^T(\boldsymbol{x}), \tag{3}$$

$$\alpha_1 \boldsymbol{a}^T\boldsymbol{a} \geq \boldsymbol{a}^T\boldsymbol{A}(\boldsymbol{x})\boldsymbol{a} \geq \alpha_0 \boldsymbol{a}^T\boldsymbol{a}, \quad \alpha_1 \geq \alpha_0 > 0, \quad \forall \boldsymbol{a} \in \mathbb{R}^d,$$

a.e. in Ω.

The boundary $\partial\Omega$ consists of disjoint parts, Γ_D on which Dirichlet conditions are imposed, and Γ_N on which Neumann conditions are imposed: $\Gamma_D \cap \Gamma_N = \varnothing$, $\Gamma_D \cup \Gamma_N = \partial\Omega$, and *meas* $\Gamma_D > 0$. The inflow Γ_- and outflow Γ_+ parts of the boundary are defined as follows:

$$\Gamma_D \supseteq \Gamma_- = \{\boldsymbol{x} \in \partial\Omega \,|\, (\boldsymbol{\beta}\cdot\boldsymbol{n})(\boldsymbol{x}) < 0 \quad \text{a.e.}\}, \qquad \Gamma_+ = \partial\Omega \backslash \Gamma_-.$$

2.1. Families of regular partitions

Let us first introduce regular partitions of Ω [20–22] (see Figure 2). Let $\mathscr{P} = \{\mathscr{P}_h(\Omega)\}_{h>0}$ be a family of regular partitions of $\Omega \subset \mathbb{R}^d$ into $N \doteq N(\mathscr{P}_h)$ subdomains Ω_e, such that for $\mathscr{P}_h \in \mathscr{P}$,

$$\bar{\Omega} = \bigcup_{e=1}^{N(\mathscr{P}_h)} \bar{\Omega}_e \quad \text{and} \quad \Omega_e \cap \Omega_f = \varnothing \quad \text{for } e \neq f. \tag{4}$$

Let us define the *inter-element boundary* by

$$\Gamma_{\text{int}} = \bigcup_{\Omega_f,\, \Omega_e \in \mathscr{P}_h} (\partial\Omega_f \cap \partial\Omega_e). \tag{5}$$

On Γ_{int}, we define $\boldsymbol{n} = \boldsymbol{n}_e$ on $(\partial\Omega_e \cap \partial\Omega_f) \subset \Gamma_{\text{int}}$ for indices e and f such that $e > f$.

2.2. Broken spaces

We define the so-called *broken spaces* on the partition $\mathscr{P}_h(\Omega)$:

$$H^m(\mathscr{P}_h) = \{v \in L^2(\Omega):\ v|_{\Omega_e} \in H^m(\Omega_e) \quad \forall \Omega_e \in \mathscr{P}_h(\Omega)\}, \tag{6}$$

if $v \in H^m(\Omega_e)$, the extension of v to the boundary $\partial\Omega_e$, indicated by the trace operation $\gamma_0 v$, is such that $\gamma_0 v \in H^{m-1/2}(\partial\Omega_e)$, $m \geq 1/2$. The trace of the normal derivative $\gamma_1 v \in H^{m-3/2}(\partial\Omega_e)$, $m > 3/2$, which will be written as $\nabla v \cdot \boldsymbol{n}|_{\partial\Omega_e}$, is interpreted as a generalized flux at the element boundary $\partial\Omega_e$.

With this notation, for $v|_{\Omega_e} \in H^{3/2+\epsilon}(\Omega_e)$ and $v|_{\Omega_f} \in H^{3/2+\epsilon}(\Omega_f)$, we introduce the *jump operator* $[\,\cdot\,]$ defined on $\Gamma_{ef} = \bar{\Omega}_e \cap \bar{\Omega}_f \neq \varnothing$ as follows:

$$[v] = (\gamma_0 v)|_{\partial\Omega_e \cap \Gamma_{ef}} - (\gamma_0 v)|_{\partial\Omega_f \cap \Gamma_{ef}}, \quad e > f, \tag{7}$$

and the *average operator* $\langle\,\cdot\,\rangle$ for the normal flux is defined for $(\boldsymbol{A}\nabla v)\cdot\boldsymbol{n} \in L^2(\Gamma_{ef})$ as

$$\langle (\boldsymbol{A}\nabla v)\cdot \boldsymbol{n}\rangle = \frac{1}{2}\left(((\boldsymbol{A}\nabla v)\cdot \boldsymbol{n})\big|_{\partial\Omega_e \cap \Gamma_{ef}} + ((\boldsymbol{A}\nabla v)\cdot \boldsymbol{n})\big|_{\partial\Omega_f \cap \Gamma_{ef}}\right), \quad e > f, \tag{8}$$

where $\boldsymbol{A}$ is the diffusivity. Note that $\boldsymbol{n}$ represents the outward normal of the element with higher index.

3. THE DISCONTINUOUS GALERKIN METHOD

The discontinuous Galerkin formulation for convection–diffusion problems is built as an extension of the classical discontinuous Galerkin method for hyperbolic problems [23–31], with the diffusion operators treated as in [7–9]. Here we review definitions and formulations presented in [8].

3.1. Weak formulation

Let $W(\mathscr{P}_h)$ be the Hilbert space on the partition $\mathscr{P}_h$ defined as the completion of $H^{3/2+\epsilon}(\mathscr{P}_h)$ under the norm $\|\cdot\|_W$ defined as follows (induced by (14)):

$$\|u\|_W^2 = \|u\|_V^2 + \|u\|_\beta^2 + \|u\sigma^{1/2}\|_{0,\Omega}^2, \tag{9}$$

$$\|v\|_V^2 = \sum_{\Omega_e \in \mathscr{P}_h} \int_{\Omega_e} \nabla v \cdot \boldsymbol{A}\nabla v \, \mathrm{d}x + |v|_{0,\Gamma_{\mathscr{P}_h}}^2, \tag{10}$$

$$\begin{aligned}\|u\|_\beta^2 = {} & |u|\boldsymbol{\beta}|^{1/2}|_{0,\Omega}^2 + \sum_{\Omega_e \in \mathscr{P}_h} |\nabla u\cdot\boldsymbol{\beta}/|\boldsymbol{\beta}|^{1/2}|_{0,\Omega_e}^2 + |u|\boldsymbol{\beta}\cdot\boldsymbol{n}|^{1/2}|_{0,\Gamma_+}^2 + |h^\alpha u^- |\boldsymbol{\beta}\cdot\boldsymbol{n}|^{1/2}|_{0,\Gamma_{\mathrm{int}}}^2 \\ & + |h^{-\alpha}[u]|\boldsymbol{\beta}\cdot\boldsymbol{n}|^{1/2}|_{0,\Gamma_{\mathrm{int}}}^2,\end{aligned} \tag{11}$$

$$|v|_{0,\Gamma_{\mathscr{P}_h}}^2 = |h^{-\alpha}v|_{0,\Gamma_{\mathrm{D}}}^2 + |h^\alpha(\boldsymbol{A}\nabla v)\cdot\boldsymbol{n}|_{0,\Gamma_{\mathrm{D}}}^2 + |h^{-\alpha}[v]|_{0,\Gamma_{\mathrm{int}}}^2 + |h^\alpha\langle(\boldsymbol{A}\nabla v)\cdot\boldsymbol{n}\rangle|_{0,\Gamma_{\mathrm{int}}}^2, \tag{12}$$

and

$$|v|_{0,\Gamma}^2 = \int_\Gamma v^2 \, \mathrm{d}s, \quad \text{for } \Gamma \in \{\Gamma_{\mathrm{D}}, \Gamma_{\mathrm{N}}, \Gamma_{\mathrm{int}}\}.$$

The terms $h^{\pm\alpha}$, with $\alpha = 1/2$, are introduced to minimize the mesh-dependence of an otherwise mesh-dependent norm. In (12), the value of h is $h_e/(2\alpha_1)$ on Γ_{D}, and the average $(h_e + h_f)/(2\alpha_1)$ on that part of Γ_{int} shared by two generic elements Ω_e and Ω_f, the constant α_1 being defined in (3). In (11), however, h is $h_e/2$ on Γ_{D}, and the average $(h_e + h_f)/2$ on $\partial\Omega_e \cap \partial\Omega_f$.

A consistent formulation of the problem in (1) and (2) is the following variational statement:

$$\boxed{\text{Find } u \in W(\mathscr{P}_h) \text{ such that} \quad B(u, v) = L(v) \quad \forall v \in W(\mathscr{P}_h)} \tag{13}$$

where

$$\begin{aligned}B(u, v) = {} & \sum_{\Omega_e \in \mathscr{P}_h} \left\{ \int_{\Omega_e} [\nabla v \cdot \boldsymbol{A}\nabla u - (\nabla v\cdot\boldsymbol{\beta})u + v\sigma u] \, \mathrm{d}\mathbf{x} + \int_{\partial\Omega_e \setminus \Gamma_-} v u^- (\boldsymbol{\beta}\cdot\boldsymbol{n}_e) \, \mathrm{d}\mathbf{s} \right\} \\ & + \int_{\Gamma_{\mathrm{D}}} ((\boldsymbol{A}\nabla v)\cdot\boldsymbol{n} u - v(\boldsymbol{A}\nabla u)\cdot\boldsymbol{n}) \, \mathrm{d}\mathbf{s} + \int_{\Gamma_{\mathrm{int}}} (\langle(\boldsymbol{A}\nabla v)\cdot\boldsymbol{n}\rangle[u] - \langle(\boldsymbol{A}\nabla u)\cdot\boldsymbol{n}\rangle[v]) \, \mathrm{d}\mathbf{s},\end{aligned} \tag{14}$$

$$u^\pm = \lim_{\epsilon \to 0} u(\boldsymbol{x} \pm \epsilon\boldsymbol{\beta}), \quad \text{for } \boldsymbol{x} \in \Gamma_{\mathrm{int}},$$

and

$$L(v) = \sum_{\Omega_e \in \mathscr{P}_h} \int_{\Omega_e} vS \, \mathrm{d}\mathbf{x} + \int_{\Gamma_D} (\boldsymbol{A}\nabla v)\cdot \boldsymbol{n} f \, \mathrm{d}\mathbf{s} + \int_{\Gamma_N} vg \, \mathrm{d}\mathbf{s} - \int_{\Gamma_-} vf(\boldsymbol{\beta}\cdot\boldsymbol{n}) \, \mathrm{d}\mathbf{s}. \tag{15}$$

Remark

Note that $H_0^1(\Omega) \subset W(\mathscr{P}_h)$. Indeed, for $u, v \in H_0^1(\Omega)$, the bilinear and linear forms $B(u, v)$ and $L(v)$ reduce to those of the continuous Galerkin formulation, which is known to be unstable for not well-resolved convection-dominated problems. The use of discontinuous basis functions in combination with (14) and (15), however, produces a method with superior stability properties. It is proven in Reference [8] that the formulation presented is globally and locally (elementwise) conservative.

3.2. Polynomial approximations on partitions

For future reference, we record a local approximation property of polynomial finite element approximations. Let $\hat{\Omega}$ be a regular master element in $\mathbb{R}^d$, and let $\{F_{\Omega_e}\}$ be a family of invertible maps from $\hat{\Omega}$ onto Ω_e (see Figure 3). For every element $\Omega_e \in \mathscr{P}_h$, the finite-dimensional space of real-valued shape functions $\hat{P} \subset H^m(\hat{\Omega})$ is the space $P_{p_e}(\hat{\Omega})$ of polynomials of degree $\leq p_e$ defined on $\hat{\Omega}$. Then we define

$$P_{p_e}(\Omega_e) = \{\psi \,|\, \psi = \hat{\psi} \circ F_{\Omega_e}^{-1},\ \hat{\psi} \in \hat{P} = P_{p_e}(\hat{\Omega})\}. \tag{16}$$

Using the spaces $P_{p_e}(\Omega_e)$, we can define

$$W_p(\mathscr{P}_h) = \prod_{e=1}^{N(\mathscr{P}_h)} P_{p_e}(\Omega_e), \tag{17}$$

$N(\mathscr{P}_h)$ being the number of elements in $\mathscr{P}_h$.

The approximation properties of $W_p(\mathscr{P}_h)$ will be estimated using standard local approximation estimates (see [32]). Let $u \in H^s(\Omega_e)$; there exists a constant C depending on s and on the

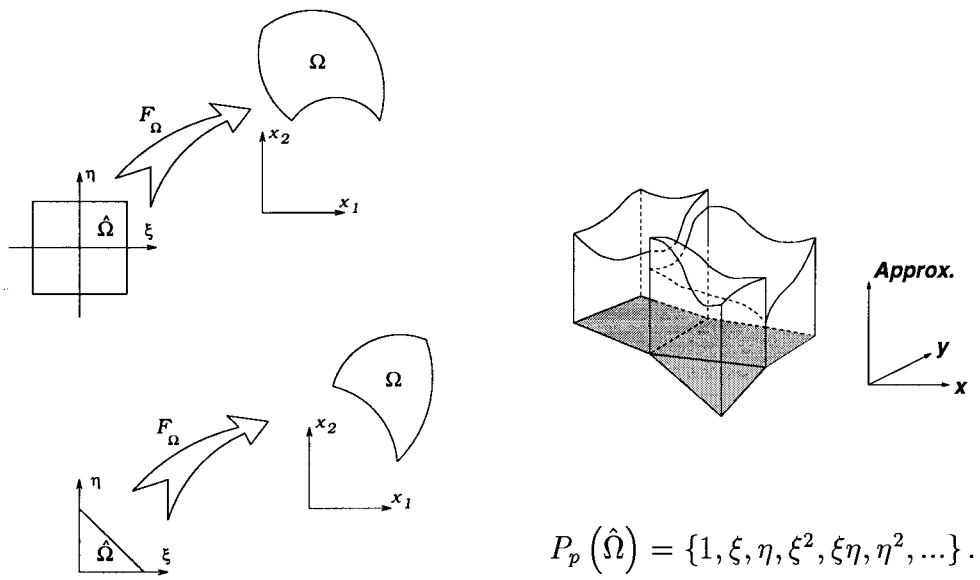

Figure 3. Mappings $\hat{\Omega} \to \Omega_e$ and discontinuous approximation.

angle condition of Ω_e, but independent of u, $h_e = \mathrm{diam}(\Omega_e)$, and p_e, and a polynomial u_p of degree p_e, such that for any $0 \le r \le s$, the following estimate holds:

$$\|u - u_p\|_{r,\Omega_e} \le C \frac{h_e^{\mu - r}}{p_e^{s-r}} \|u\|_{s,\Omega_e}, \quad s \ge 0, \tag{18}$$

where $\|\cdot\|_{r,\Omega_e}$ denotes the usual Sobolev norm, and $\mu = \min(p_e + 1, s)$.

3.3. Discontinuous Galerkin approximation

The variational formulation of the discontinuous Galerkin method (13) will be used as a basis to construct approximations to the exact solution in a finite-dimensional space. The variational formulation in the space $W_p(\mathscr{P}_h)$ is the following:

$$\boxed{\text{Find } u_{\mathrm{DG}} \in W_p(\mathscr{P}_h) \text{ such that } \quad B(u_{\mathrm{DG}}, v_h) = L(v_h) \quad \forall v_h \in W_p(\mathscr{P}_h)} \tag{19}$$

where $B(\,.\,,.\,)$ and $L(\,\cdot\,)$ are defined in (14) and (15) respectively.

Note that all the properties of the discontinuous Galerkin method (13) also hold for the finite-dimensional approximation (19); namely, solutions are elementwise conservative, mass matrices are block diagonal, and the space of discontinuous functions provides the basis to obtain solutions with potentially good stability properties.

One of the most important characteristics of a method for the solution of convection–diffusion problems is that of stability. The following section addresses this issue and provides an *a priori* error estimation to solutions of (19).

3.4. A priori error estimation

Let us first define the norm $\|\cdot\|_{W_1}$ which is used in the error estimate:

$$\|u\|_{W_1}^2 = \|u\|_{V_1}^2 + \|u\|_{\beta_1}^2, \tag{20}$$

$$\|u\|_{V_1}^2 = |u|_{0,\mathscr{P}_h}^2 + |h^\alpha u|_{0,\Gamma_{\mathrm{D}} \cup \Gamma_{\mathrm{N}}}^2 + |h^\delta \alpha_1^{-1} (\boldsymbol{A}\nabla u)\cdot \boldsymbol{n}|_{0,\Gamma_{\mathrm{D}}}^2 + |h^\alpha [u]|_{0,\Gamma_{\mathrm{int}}}^2 + |h^\delta \alpha_1^{-1} \langle (\boldsymbol{A}\nabla u)\cdot \boldsymbol{n}\rangle|_{0,\Gamma_{\mathrm{int}}}^2 + |h^\alpha \langle u \rangle|_{0,\Gamma_{\mathrm{int}}}^2, \tag{21}$$

$$|u|_{0,\mathscr{P}_h}^2 = \sum_{\Omega_e \in \mathscr{P}_h} \int_{\Omega_e} u^2 \, \mathrm{d}\mathbf{x}, \qquad |v|_{0,\Gamma}^2 = \int_\Gamma v^2 \, \mathrm{d}\mathbf{s}, \quad \text{for } \Gamma \in \{\Gamma_{\mathrm{D}}, \Gamma_{\mathrm{N}}, \Gamma_{\mathrm{int}}\},$$

and

$$\|u\|_{\beta_1}^2 = |h^\alpha u^+|_{0,\Gamma_-}^2 + |h^\alpha [u]|_{0,\Gamma_{\mathrm{int}}}^2 + \|h u_\beta\|_{0,\Omega}^2, \tag{22}$$

with $\alpha = 1/2$, $\delta = 3/2$ and $u_\beta = |\boldsymbol{\beta}|^{-1}(\nabla u \cdot \boldsymbol{\beta})$ when $|\boldsymbol{\beta}| > 0$, otherwise $u_\beta = 0$. In $\|\cdot\|_{V_j}$ and $\|\cdot\|_{\beta_j}$, the scaling parameter h is $h_e/2$ on $\partial\Omega_e \cap \partial\Omega$, and the average $(h_e + h_f)/2$ on $\partial\Omega_e \cap \partial\Omega_f$.

Solutions to convection–diffusion problems can exhibit features that range from those of diffusion-dominated problems to those of pure convection problems. The error of diffusion-dominated problems is better measured in the H^1-norm because the associated physics depends on the solution gradient, such as heat transfer, viscous stresses, etc.; whereas the error in convection-dominated transport is better measured in the L^2-norm because the underlying physics depends almost exclusively on the solution values rather than on its gradient.

The range $[0, 1)$ of local Peclet numbers (Pe) represents a class of problems in which diffusion effects are dominant, and for which the W-norm converges to the V-norm as $Pe \to 0$. The analysis of stability in the V-norm for diffusion dominated problems was presented in [7,9], where optimal h-convergence rates are presented.

For high *Pe*, where convection is important, the following *a priori* error estimate applies (see [8]). It is assumed that the reaction coefficient $\sigma = 0$, which is the worst case scenario from the point of view of stability.

Theorem 3.1
Let the solution to (13) be $u \in H^s(\mathscr{P}_h(\Omega))$, with $s > 3/2$, and assume that there exists $\kappa \geq 0$ and $C_p > 0$ such that

$$\inf_{\substack{u \in W_1 \\ \|u\|_{W_1} = 1}} \sup_{\substack{v \in W_1 \\ \|v\|_{W_1} \leq 1}} |B(u, v)| \geq C_p p_{\max}^{-\kappa}, \tag{23}$$

where $p_{\max} = \max_e(p_e)$. If the approximation estimate (18) holds for the spaces $W_p(\mathscr{P}_h)$, then the error of the approximate solution u_{DG} is bounded as follows:

$$\|u - u_{\mathrm{DG}}\|_{W_1}^2 \leq C p_{\max}^{2\kappa} \sum_{\Omega_e \in \mathscr{P}_h} \left(\frac{h_e^{\mu_e - \epsilon}}{p_e^{s - (3/2) - \epsilon}} \|u\|_{s, \Omega_e} \right)^2, \tag{24}$$

where $\mu_e = \min(p_e + 1, s)$, $\epsilon \to 0^+$, and the constant C depends on s and on the angle condition of the element, but it is independent of u, h_e and p_e.

A proof of this result can be found in [8].

Remark
Numerical experiments presented in [8] indicate that $\kappa < 1.5$.

4. EULER AND NAVIER–STOKES PROBLEMS

First we introduce a model problem and related notations in preparation for developing and analyzing the discontinuous Galerkin formulation.

Let Ω be a bounded Lipschitz domain in $\mathbb{R}^d$. The governing equations for the conservation of mass, momentum and energy can be written in vector form as follows:

$$\begin{aligned} &\frac{\partial \boldsymbol{U}}{\partial t} + \frac{\partial \boldsymbol{F}_i}{\partial x_i} = \frac{\partial \boldsymbol{F}_i^v}{\partial x_i} + \boldsymbol{S}, \quad \text{in } \Omega \\ &\boldsymbol{U}(\boldsymbol{x}, 0) = \boldsymbol{U}_0(\boldsymbol{x}), \qquad \text{at } t = 0 \end{aligned} \tag{25}$$

where repeated indices are summed throughout their range, $\boldsymbol{U} = (u_1, \ldots, u_m) = \boldsymbol{U}(\boldsymbol{x}, t) \in \mathbb{R}^m$ is a vector of conservation variables with $m = d + 1$ or $d + 2$ when the energy equation is included, $\boldsymbol{F}_i(\boldsymbol{U}) = (f_{1i}, \ldots, f_{mi}) \in \mathbb{R}^m$ and $\boldsymbol{F}_i^v(\boldsymbol{U}) = (f_{1i}^v, \ldots, f_{mi}^v) \in \mathbb{R}^m$ are the inviscid and diffusive flux vectors associated with the ith space co-ordinate, and $\boldsymbol{S}$ represents the body forces in the momentum equations and a source of heat (e.g. heat source due to viscous dissipation) in the energy equation. The system of equations (25) is accompanied by appropriate boundary conditions for each problem.

4.1. Inviscid and viscous flux vectors

The inviscid flux vectors $\boldsymbol{F}_i$ are homogeneous functions of degree 1 in the conservative variables $\boldsymbol{U}$; therefore, the fluxes can be written as $\boldsymbol{F}_i = \boldsymbol{A}_i(\boldsymbol{U})\boldsymbol{U}$, where $\boldsymbol{A}_i(\boldsymbol{U})$ is the Jacobian

matrix. Let $\boldsymbol{F}_n(\boldsymbol{U})$ be the normal flux at any point on a boundary $\partial\Omega$ with outward normal $\boldsymbol{n}$; then

$$\boldsymbol{F}_n = \boldsymbol{F}_i n_i, \quad i \in [1, \ldots, d],$$

$$\boldsymbol{A}_n(\boldsymbol{U}) = \frac{\partial \boldsymbol{F}_n(\boldsymbol{U})}{\partial \boldsymbol{U}} = \boldsymbol{A}_i(\boldsymbol{U}) n_i, \quad \boldsymbol{A}_n(\boldsymbol{U}) \in \mathbb{R}^m \times \mathbb{R}^m.$$

The flux vector $\boldsymbol{F}_n(\boldsymbol{U})$ can be split into inflow and outflow components $\boldsymbol{F}_n^+$ and $\boldsymbol{F}_n^-$; for example

$$\boldsymbol{F}_n^{\pm}(\boldsymbol{U}) = \boldsymbol{R}\boldsymbol{\Lambda}^{\pm}\boldsymbol{R}^{-1}\boldsymbol{U}, \quad \boldsymbol{\Lambda}^{\pm} = \frac{1}{2}(\boldsymbol{\Lambda} \pm |\boldsymbol{\Lambda}|),$$

where $\boldsymbol{\Lambda}$ is the diagonal matrix of eigenvalues of $\boldsymbol{A}_n$, and the columns of the matrix $\boldsymbol{R}$ are the corresponding eigenvectors. From a physical point of view, $\boldsymbol{F}_n^+$ and $\boldsymbol{F}_n^-$ represent the fluxes of mass, momentum and energy leaving $(+)$ and entering $(-)$ the domain through $\partial\Omega$.

Given that the approximation of field variables may be discontinuous across internal surfaces in Ω or across $\partial\Omega$, let us define

$$\boldsymbol{U}^{\pm} = \lim_{\epsilon \to 0^+} \boldsymbol{U}(\boldsymbol{x} \pm \epsilon \boldsymbol{n}),$$

where $\boldsymbol{x}$ is a point at a boundary that can be real (e.g. bounding walls) or artificial (e.g. inter-element, far-field). With this notation, $\boldsymbol{F}_n^+(\boldsymbol{U}^-)$ is the flux in the direction $\boldsymbol{n}$, and $\boldsymbol{F}_n^-(\boldsymbol{U}^+)$ is that in the opposite direction.

The projection of the viscous flux vectors $\boldsymbol{F}_i^v$ onto the normal $\boldsymbol{n}$ to a boundary is a linear functional of $\boldsymbol{U}$, and will be written in the following alternative forms

$$\boldsymbol{F}_i^v n_i = \boldsymbol{F}_n^v = \boldsymbol{D}_n \boldsymbol{U},$$

where for Newtonian flows, the matrix $\boldsymbol{D}_n$ is a linear differential operator.

5. SPACE DISCRETIZATION WITH BROKEN SPACES

For a partition $\mathscr{P}_h$ in this family, we introduce a broken space $\boldsymbol{V}(\mathscr{P}_h)$ of admissible vectors of conservation variables $\boldsymbol{U} = \boldsymbol{U}(\boldsymbol{x})$ as follows:

$$\begin{aligned}\boldsymbol{V}(\mathscr{P}_h) = \{\boldsymbol{U}:\ & \nabla \boldsymbol{U}_1 \cdot (\boldsymbol{F}^v(\boldsymbol{U}_2) - \boldsymbol{F}(\boldsymbol{U}_2)) \in L^1(\Omega_e);\\ & \boldsymbol{U}_1 \cdot (\boldsymbol{F}_{n_e}^+(\boldsymbol{U}_2^-) + \boldsymbol{F}_{n_e}^-(\boldsymbol{U}_3^+)) \in L^1(\partial\Omega_e);\\ & \boldsymbol{U}_1 \cdot \boldsymbol{D}_n^T \boldsymbol{U}_2 \in L^1(\partial\Omega_e);\ \boldsymbol{U}_1 \cdot \boldsymbol{F}_n^v(\boldsymbol{U}_2) \in L^1(\partial\Omega_e);\\ & \forall \{\boldsymbol{U}_1, \boldsymbol{U}_2, \boldsymbol{U}_3\} \in \boldsymbol{V}(\mathscr{P}_h), \quad \forall \Omega_e \in \mathscr{P}_h(\Omega)\}.\end{aligned}$$

For a given initial condition data $\boldsymbol{U}_0$, and appropriate boundary conditions, the space discretization using the discontinuous Galerkin method can be stated as follows:

Given $\boldsymbol{U}_0 = \boldsymbol{U}_0(\boldsymbol{x})$, for $t \in (0, T)$, find
$\boldsymbol{U}(\,.\,, t) \in V(\mathscr{P}_h) \times H^1(0, T)$ such that $\boldsymbol{U}(\boldsymbol{x}, 0) = \boldsymbol{U}_0(\boldsymbol{x})$, and

$$\begin{aligned}
&\int_\Omega \boldsymbol{W}^T \frac{\partial \boldsymbol{U}}{\partial t}\, d\mathbf{x} + \sum_{\Omega_e \in \mathscr{P}_h} \int_{\partial\Omega_e} \boldsymbol{W}^T (\boldsymbol{F}^+_{n_e}(\boldsymbol{U}^-) + \boldsymbol{F}^-_{n_e}(\boldsymbol{U}^+))\, d\mathbf{s} \\
&+ \int_{\Gamma_{\text{int}}} (\langle \boldsymbol{W}^T \boldsymbol{D}^T_n \rangle [\boldsymbol{U}] - [\boldsymbol{W}^T] \langle \boldsymbol{F}^v_n \rangle)\, d\mathbf{s} + \int_{\Gamma_D} (\boldsymbol{W}^T \boldsymbol{D}^T_n \boldsymbol{U} - \boldsymbol{W}^T \boldsymbol{F}^v_n)\, d\mathbf{s} \\
&+ \sum_{\Omega_e \in \mathscr{P}_h} \int_{\partial\Omega_e} \frac{\partial \boldsymbol{W}^T}{\partial x_i} (\boldsymbol{F}^v_i - \boldsymbol{F}_i)\, d\mathbf{x} \\
&- \int_\Omega \boldsymbol{W}^T \boldsymbol{S}\, d\mathbf{x} + \int_{\Gamma_D} \boldsymbol{W}^T \boldsymbol{D}^T_n \hat{\boldsymbol{U}}\, d\mathbf{s} + \int_{\Gamma_N} \boldsymbol{W}^T \hat{\boldsymbol{F}}^v_n\, d\mathbf{s}, \quad \forall \boldsymbol{W} \in \boldsymbol{V}(\mathscr{P}_h)
\end{aligned} \tag{26}$$

where

$$\boldsymbol{F}_{n_e}(\boldsymbol{U}) = \boldsymbol{F}_i(\boldsymbol{U}) n_{e_i}, \qquad \boldsymbol{U}^\pm = \lim_{\epsilon \to 0^+} \boldsymbol{U}(\boldsymbol{x} \pm \epsilon \boldsymbol{n}_e), \qquad \boldsymbol{F}^v_n(\boldsymbol{U}) = \boldsymbol{F}^v_i(\boldsymbol{U}) n_i, \qquad \boldsymbol{F}^v_n(\boldsymbol{U}) = \boldsymbol{D}_n \boldsymbol{U}.$$

$\boldsymbol{F}^\pm_n$ are known in closed form for the usual flux vector and flux difference splittings (see [7] and references therein).

It is important to observe that (26) reduces to the classical weak Galerkin approximation if we restrict $\boldsymbol{V}(\mathscr{P}_h)$ to a space of continuous functions.

We now prove that (26) renders a *conservative* formulation. To show that (26) is *globally conservative*, let us pick a test function $\boldsymbol{W} = (v_1, \ldots, v_m)$ such that

$$v_i(\boldsymbol{x}) = 1, \quad i = 1, \ldots, m \quad \forall \boldsymbol{x} \in \Omega,$$

by definition $\boldsymbol{W} \in \boldsymbol{V}(\mathscr{P}_h)$. Substituting $\boldsymbol{W}$ in (26), we get

$$\int_\Omega \frac{\partial \boldsymbol{U}}{\partial t}\, d\mathbf{x} + \sum_{\Omega_e \in \mathscr{P}_h} \int_{\partial\Omega_e} (\boldsymbol{F}^+_{n_e}(\boldsymbol{U}^-) + \boldsymbol{F}^-_{n_e}(\boldsymbol{U}^+))\, d\mathbf{s} - \int_{\Gamma_D} \boldsymbol{F}^v_n\, d\mathbf{s} = \int_\Omega \boldsymbol{S}\, d\mathbf{x} + \int_{\Gamma_N} \hat{\boldsymbol{F}}^v_n\, d\mathbf{s}. \tag{27}$$

For any pair of adjoining elements (Ω_e, Ω_f), the following identities hold:

$$\boldsymbol{F}^+_{n_e}(\boldsymbol{U}^-) = -\boldsymbol{F}^-_{n_f}(\boldsymbol{U}^+) \quad \text{and} \quad \boldsymbol{F}^-_{n_e}(\boldsymbol{U}^+) = -\boldsymbol{F}^+_{n_f}(\boldsymbol{U}^-).$$

Substituting the above identities in (27), we obtain

$$\int_\Omega \frac{\partial \boldsymbol{U}}{\partial t}\, d\mathbf{x} + \int_{\partial\Omega} (\boldsymbol{F}^+_n(\boldsymbol{U}^-) + \boldsymbol{F}^-_n(\boldsymbol{U}^+))\, d\mathbf{s} = \int_\Omega \boldsymbol{S}\, d\mathbf{x} + \int_{\Gamma_N} \hat{\boldsymbol{F}}^v_n\, d\mathbf{s} + \int_{\Gamma_D} \boldsymbol{F}^v_n\, d\mathbf{s}, \tag{28}$$

which shows that the formulation is globally conservative.

To show that the formulation is also *locally conservative*, we select a generic weighting function

$$\boldsymbol{W} = (v_1, \ldots, v_m) \in \boldsymbol{V}(\mathscr{P}_h) \quad \text{such that } v_i(\boldsymbol{x}) = \begin{cases} 1 & \boldsymbol{x} \in \Omega_e \\ 0 & \boldsymbol{x} \notin \Omega_e \end{cases}, \quad i = 1, \ldots, m,$$

and substituting $\boldsymbol{W}$ in (26), we get

$$\begin{aligned}
&\int_{\Omega_e} \frac{\partial \boldsymbol{U}}{\partial t}\, d\mathbf{x} + \int_{\partial\Omega_e} (\boldsymbol{F}^+_{n_e}(\boldsymbol{U}^-) + \boldsymbol{F}^-_{n_e}(\boldsymbol{U}^+))\, d\mathbf{s} \\
&= \int_{\Omega_e} \boldsymbol{S}\, d\mathbf{x} + \int_{\partial\Omega_e \cap \Gamma_N} \hat{\boldsymbol{F}}^v_n + \int_{\partial\Omega_e \cap \Gamma_D} \boldsymbol{F}^v_n\, d\mathbf{s} + \int_{\partial\Omega_e \cap \Gamma_{\text{int}}} \langle \boldsymbol{F}^v_n \rangle\, d\mathbf{s},
\end{aligned}$$

which represents the conservation equations at *element* level when the inter-element viscous forces are taken as the average $\langle \boldsymbol{F}_n^v \rangle$.

5.1. Equivalence of the weak formulation

In this section we prove that any solution to problem (25) with appropriate boundary conditions is also a solution to the variational problem (26).

Assuming that the fluxes $\boldsymbol{F}_i^v$ and $\boldsymbol{F}_i$ are differentiable within each element of the partition, we rewrite the summations on the left-hand-side of (26) as follows:

$$\sum_{\Omega_e \in \mathscr{P}_h} \int_{\Omega_e} \frac{\partial \boldsymbol{W}^T}{\partial x_i} (\boldsymbol{F}_i^v - \boldsymbol{F}_i)\, \mathrm{d}\mathbf{x} = -\sum_{\Omega_e \in \mathscr{P}_h} \int_{\Omega_e} \boldsymbol{W}^T \left(\frac{\partial \boldsymbol{F}_i^v}{\partial x_i} - \frac{\partial \boldsymbol{F}_i}{\partial x_i} \right) \mathrm{d}\mathbf{x} + \int_{\partial\Omega} \boldsymbol{W}^T (\boldsymbol{F}_n^v - \boldsymbol{F}_n)\, \mathrm{d}\mathbf{s} + \int_{\Gamma_{\mathrm{int}}} [\boldsymbol{W}^T (\boldsymbol{F}_n^v - \boldsymbol{F}_n)]\, \mathrm{d}\mathbf{s}$$

and

$$\sum_{\Omega_e \in \mathscr{P}_{\mathrm{p}}} \int_{\partial\Omega_e} \boldsymbol{W}^T (\boldsymbol{F}_{n_e}^+(\boldsymbol{U}^-) + \boldsymbol{F}_{n_e}^-(\boldsymbol{U}^+))\, \mathrm{d}\mathbf{x} = \int_{\partial\Omega} \boldsymbol{W}^T (\boldsymbol{F}_n^+(\boldsymbol{U}^-) + \boldsymbol{F}_n^-(\boldsymbol{U}^+))\, \mathrm{d}\mathbf{s} + \int_{\Gamma_{\mathrm{int}}} [\boldsymbol{W}^T] (\boldsymbol{F}_n^+(\boldsymbol{U}^-) + \boldsymbol{F}_n^-(\boldsymbol{U}^+))\, \mathrm{d}\mathbf{s}.$$

Substituting the above expressions in (26), we obtain

$$\int_{\partial\Omega} \boldsymbol{W}^T (\boldsymbol{F}_n^+(\boldsymbol{U}^-) + \boldsymbol{F}_n^-(\boldsymbol{U}^+) - \boldsymbol{F}_n)\, \mathrm{d}\mathbf{s} + \int_{\Gamma_{\mathrm{D}}} \boldsymbol{W}^T \boldsymbol{D}_n^T (\boldsymbol{U} - \hat{\boldsymbol{U}})\, \mathrm{d}\mathbf{s} + \int_{\Gamma_{\mathrm{N}}} \boldsymbol{W}^T (\boldsymbol{F}_n^v - \hat{\boldsymbol{F}}_n^v)\, \mathrm{d}\mathbf{s}$$
$$+ \int_{\Gamma_{\mathrm{int}}} \langle \boldsymbol{W}^T \boldsymbol{D}_n^T \rangle [\boldsymbol{U}]\, \mathrm{d}\mathbf{s} + \int_{\Gamma_{\mathrm{int}}} \{ [\boldsymbol{W}^T] (\boldsymbol{F}_n^+(\boldsymbol{U}^-) + \boldsymbol{F}_n^-(\boldsymbol{U}^+) - \langle \boldsymbol{F}_n \rangle) - \langle \boldsymbol{W}^T \rangle [\boldsymbol{F}_n - \boldsymbol{F}_n^v] \}\, \mathrm{d}\mathbf{s}$$
$$+ \sum_{\Omega_e \in \mathscr{P}_h} \int_{\Omega_e} \boldsymbol{W}^T \left(\frac{\partial \boldsymbol{U}}{\partial t} + \frac{\partial \boldsymbol{F}_i}{\partial x_i} - \frac{\partial \boldsymbol{F}_i^v}{\partial x_i} - \boldsymbol{S} \right) \mathrm{d}\mathbf{x} = 0, \quad \forall \boldsymbol{W} \in \boldsymbol{V}(\mathscr{P}_h),$$

which shows that any sufficiently smooth solution to the model problem (25) with appropriate boundary conditions satisfies (26).

6. APPROXIMATION WITH POLYNOMIAL BASIS

For every element $\Omega_e \in \mathscr{P}_h$, the finite-dimensional space of real-valued shape functions is taken to be the space $P_{p_e}(\hat{\Omega})$ of polynomials of degree $\leq p_e$ defined on its master element $\hat{\Omega}$. Then we define

$$P_{p_e}(\Omega_e) = \{ \psi \,|\, \psi = \hat{\psi} \circ F_{\Omega_e}^{-1},\ \hat{\psi} \in \hat{P} = P_{p_e}(\hat{\Omega}) \}, \tag{29}$$

where F_{Ω_e} is an invertible mapping from the master element $\hat{\Omega}$ onto Ω_e.

Let $\boldsymbol{V}_p(\mathscr{P}_h)$ be the following finite-dimensional subspace of $\boldsymbol{V}(\mathscr{P}_h)$:

$$\boldsymbol{V}_p(\mathscr{P}_h) = \left(\prod_{e=1}^{N(\mathscr{P}_h)} P_{p_e}(\Omega_e) \right)^m \subset \boldsymbol{V}(\mathscr{P}_h),$$

and let the time domain be subject to a family of partitions:

$$\mathscr{P}_t(t_0, t_N) = \{ (t_i, t_{i+1}),\ t_i < t_{i+1},\ 0 \leq i \leq N-1 \}.$$

Then, a space–time discretization of the Navier–Stokes equations with piecewise constant approximation in time can be stated as follows:

$$
\begin{aligned}
&\text{Given } \boldsymbol{U}_0 = \boldsymbol{U}_0(\boldsymbol{x}), \text{ find } \boldsymbol{U}_h \in \boldsymbol{V}_p(\mathscr{P}_h) \times \boldsymbol{V}_0(\mathscr{P}_t), \text{ such that} \\
&(t_{n+1} - t_n)^{-1} \sum_{\Omega_e \in \mathscr{P}_h} \int_{\Omega_e} \boldsymbol{W}_h^T (\boldsymbol{U}_h(t_{n+1}) - \boldsymbol{U}_h(t_n))\, \mathrm{d}\mathbf{x} \\
&+ \sum_{\Omega_e \in \mathscr{P}_h} \int_{\partial\Omega_e} \boldsymbol{W}_h^T (\boldsymbol{F}_{n_e}^+(\boldsymbol{U}_h^-(t_n)) + \boldsymbol{F}_{n_e}^-(\boldsymbol{U}_h^+(t_n)))\, \mathrm{d}\mathbf{s} \\
&+ \int_{\Gamma_{\mathrm{int}}} (\langle \boldsymbol{W}_h^T \boldsymbol{D}_n^T \rangle [\boldsymbol{U}_h(t_n)] - [\boldsymbol{W}_h^T] \langle \boldsymbol{F}_n^v(t_n) \rangle)\, \mathrm{d}\mathbf{s} + \int_{\Gamma_{\mathrm{D}}} (\boldsymbol{W}_h^T \boldsymbol{D}_n^T \boldsymbol{U}_h - \boldsymbol{W}_h^T \boldsymbol{F}_n^v)\, \mathrm{d}\mathbf{s} \\
&+ \sum_{\Omega_e \in \mathscr{P}_h} \int_{\partial\Omega_e} \frac{\partial \boldsymbol{W}_h^T}{\partial x_i} (\boldsymbol{F}_i^v - \boldsymbol{F}_i)(t_n)\, \mathrm{d}\mathbf{x} \\
&= \sum_{\Omega_e \in \mathscr{P}_h} \int_{\Omega_e} \boldsymbol{W}_h^T \boldsymbol{S}(t_n)\, \mathrm{d}\mathbf{x} + \int_{\Gamma_{\mathrm{D}}} \boldsymbol{W}_h^T \boldsymbol{D}_n^T \hat{\boldsymbol{U}}(t_n)\, \mathrm{d}\mathbf{s} + \int_{\Gamma_{\mathrm{N}}} \boldsymbol{W}_h^T \hat{\boldsymbol{F}}_n^v(t_n)\, \mathrm{d}\mathbf{s} \\
&\forall \boldsymbol{W}^h \in \boldsymbol{V}_p(\mathscr{P}_h), \quad 0 \le n \le N-1
\end{aligned}
\tag{30}
$$

This discretization is only first-order-accurate in time, it is used to converge to steady solutions of the Navier–Stokes equations.

Regarding the space $\boldsymbol{V}_p(\mathscr{P}_h)$, analytical stability studies and numerical experiments presented in [6,7,9] indicate that the order of polynomial approximation should be $p_e \ge 2$ $\forall \Omega_e \in \mathscr{P}_h(\Omega)$.

6.1. Algorithm for steady state computations

Let the restriction of the state vector $\boldsymbol{U}_h$ to any given element Ω_e be written as

$$\boldsymbol{U}_h(\boldsymbol{x}, t)|_{\Omega_e} = \boldsymbol{W}_e(\boldsymbol{x}) \boldsymbol{u}_e(t),$$

where $\boldsymbol{W}_e$ is a matrix of local shape functions of dimension $m \times (P_{p_e}(\Omega_e))^m$, and $\boldsymbol{u}_e$ is the vector of element degrees of freedom of dimension $(P_{p_e}(\Omega_e))^m$. Then, the algebraic system of equations (30) can be written in matrix form as follows:

$$\boldsymbol{M} \delta \boldsymbol{u} = \delta t (\boldsymbol{S}^n - \boldsymbol{N}(\boldsymbol{U}^n)) \tag{31}$$

where

$$
\begin{aligned}
&\delta \boldsymbol{u} = \boldsymbol{u}^{n+1} - \boldsymbol{u}^n, \qquad \delta t = t_{n+1} - t_n, \qquad \boldsymbol{M} = \sum_{\Omega_e \in \mathscr{P}_h} \int_{\Omega_e} \boldsymbol{W}_e^T \boldsymbol{W}_e\, \mathrm{d}\mathbf{x}, \\
&\boldsymbol{S}^n = \sum_{\Omega_e \in \mathscr{P}_h} \int_{\Omega_e} \boldsymbol{W}_e^T \boldsymbol{S}(t_n)\, \mathrm{d}\mathbf{x} + \int_{\Gamma_{\mathrm{D}}} \boldsymbol{W}^T \boldsymbol{D}_n^T \hat{\boldsymbol{U}}(t_n)\, \mathrm{d}\mathbf{s} + \int_{\Gamma_{\mathrm{N}}} \boldsymbol{W}^T \hat{\boldsymbol{F}}_n^v(t_n)\, \mathrm{d}\mathbf{s}, \\
&\boldsymbol{N}(\boldsymbol{U}^n) = \sum_{\Omega_e \in \mathscr{P}_h} \int_{\partial\Omega_e} \boldsymbol{W}_e^T (\boldsymbol{F}_{n_e}^+(\boldsymbol{U}_h^-(t_n)) + \boldsymbol{F}_{n_e}^-(\boldsymbol{U}_h^+(t_n)))\, \mathrm{d}\mathbf{s} \\
&\qquad + \int_{\Gamma_{\mathrm{int}}} (\langle \boldsymbol{W}^T \boldsymbol{D}_n^T \rangle [\boldsymbol{U}_h(t_n)] - [\boldsymbol{W}^T] \langle \boldsymbol{F}_n^v(t_n) \rangle)\, \mathrm{d}\mathbf{s} + \int_{\Gamma_{\mathrm{D}}} (\boldsymbol{W}^T \boldsymbol{D}_n^T \boldsymbol{U}_h - \boldsymbol{W}^T \boldsymbol{F}_n^v)\, \mathrm{d}\mathbf{s} \\
&\qquad + \sum_{\Omega_e \in \mathscr{P}_h} \int_{\Omega_e} \frac{\partial \boldsymbol{W}_e^T}{\partial x_i} (\boldsymbol{F}_i^v - \boldsymbol{F}_i)(t_n)\, \mathrm{d}\mathbf{x},
\end{aligned}
$$

where $\boldsymbol{W}$ is a matrix of dimension $m \times \dim(\boldsymbol{V}_p(\mathscr{P}_h))$, the mass matrix has dimensions $\dim(\boldsymbol{V}_p(\mathscr{P}_h)) \times \dim(\boldsymbol{V}_p(\mathscr{P}_h))$, whereas $\delta\boldsymbol{u}$, $\boldsymbol{S}^n$ and $\boldsymbol{N}(\boldsymbol{U}^n)$ are vectors of dimension $\dim(\boldsymbol{V}_p(\mathscr{P}_h))$.

Given that $\boldsymbol{M}$ is a block diagonal matrix with uncoupled blocks, each block having dimensions $(\dim(P_{p_e}(\Omega_e)))^m \times (\dim(P_{p_e}(\Omega_e)))^m$, the system of equations (31) can be solved element by element as follows:

$$\boxed{\begin{aligned} &\boldsymbol{M}_e \delta\boldsymbol{u}_e = \delta t(\boldsymbol{S}_e^n - \boldsymbol{N}_e(\boldsymbol{U}^n)), \\ &\boldsymbol{u}_e^{n+1} = \boldsymbol{u}_e^n + \delta\boldsymbol{u}_e \end{aligned}} \tag{32}$$

where $\boldsymbol{S}_e^n$ and $\boldsymbol{N}_e(\boldsymbol{U}^n)$ are the components of $\boldsymbol{S}^n$ and $\boldsymbol{N}(\boldsymbol{U}^n)$ associated with the test functions $\boldsymbol{W}_e$, which have local support on Ω_e.

The maximum allowable time step δt associated with an explicit time-marching scheme as (32) is limited by a CFL condition where convection is dominant, and a time step of order h^2 where diffusion effects are dominant. To ameliorate this limitation on the time step, it is advisable to utilize an elementwise point-implicit scheme.

6.2. *Elementwise point-implicit scheme*

The point-implicit scheme is obtained by linearizing all those equations coming from weight functions $\boldsymbol{W}_e$ whose support is the domain of a given element Ω_e, with respect to all the degrees of freedom $\boldsymbol{u}_e$ associated with the same element.

Using (30) with local linearization at element level, we get the following time-marching scheme:

$$\boxed{\begin{aligned} &\left(\frac{1}{\delta t}\boldsymbol{M}_e - \frac{\partial \boldsymbol{S}_e^n}{\partial \boldsymbol{u}_e} + \frac{\partial \boldsymbol{N}_e^n}{\partial \boldsymbol{u}_e}\right)\delta\boldsymbol{u}_e = (\boldsymbol{S}_e^n - \boldsymbol{N}_e(\boldsymbol{U}^n)) \\ &\boldsymbol{u}_e^{n+1} = \boldsymbol{u}_e^n + \boldsymbol{u}_e \end{aligned}} \tag{33}$$

where

$$\frac{\partial \boldsymbol{N}_e}{\partial \boldsymbol{u}_e} = \int_{\partial\Omega_e} \boldsymbol{W}_e^T \boldsymbol{A}_{n_e}^+(\boldsymbol{U}_e^-)\boldsymbol{W}_e \, \mathrm{d}\mathbf{s} + \int_{\partial\Omega_e \cap (\Gamma_{\mathrm{int}} \cup \Gamma_D)} \boldsymbol{W}_e^T(\boldsymbol{D}_n^T - \boldsymbol{D}_n)\boldsymbol{W}_e \, \mathrm{d}\mathbf{x} + \int_{\Omega_e} \frac{\partial \boldsymbol{W}_e^T}{\partial x_i}(\boldsymbol{D}_i - \boldsymbol{A}_i)(\boldsymbol{U}_e)\boldsymbol{W}_e \, \mathrm{d}\mathbf{x},$$

$$\frac{\partial \boldsymbol{S}_e^n}{\partial \boldsymbol{u}_e} = \int_{\Omega_e} \boldsymbol{W}_e^T \frac{\partial \boldsymbol{S}}{\partial \boldsymbol{U}_e}(\boldsymbol{U}^n)\boldsymbol{W}_e \, \mathrm{d}\mathbf{x},$$

and $\boldsymbol{M}_e$, $\boldsymbol{S}_e^n$ and $\boldsymbol{N}_e$ are the same as in (32).

It is important to note that the scheme is applied element by element. For steady state calculations, the changes $\delta\boldsymbol{u}_e$ are used to update $\boldsymbol{u}_e$ and to compute the residual of other elements as soon as $\delta\boldsymbol{u}_e$ is obtained. In a Gauss–Seidel fashion, this updating accelerates the convergence to the steady state.

For time-dependent problems, an explicit multi-step Runge–Kutta scheme can be applied. The number of explicit steps depends on accuracy and on stability considerations.

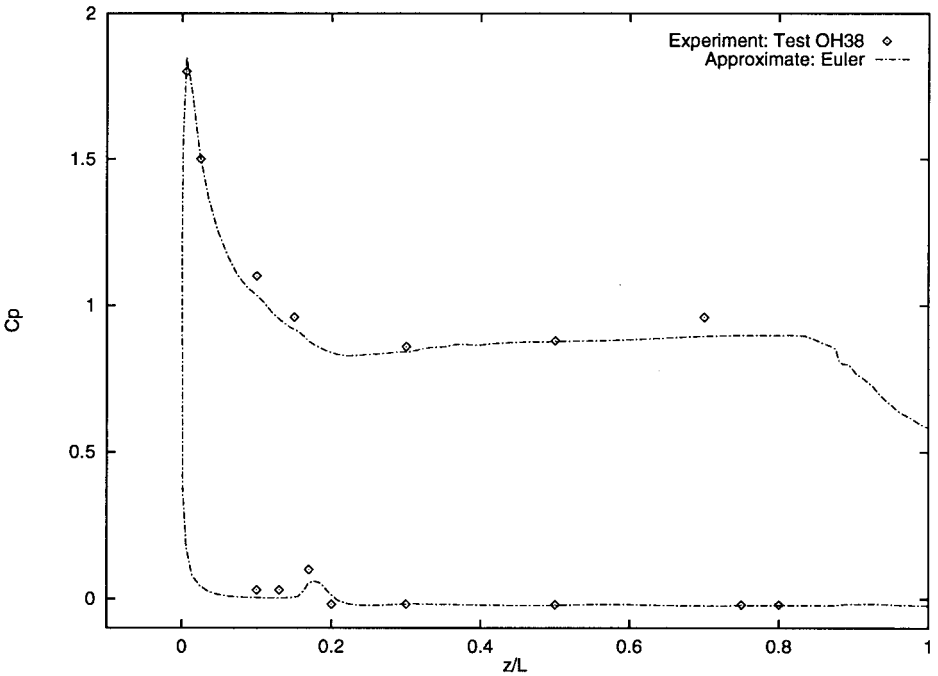

Figure 4. Pressure coefficient along the windward and leeward centerlines.

7. NUMERICAL EXPERIMENTS

The first test case is a standard benchmark for the solution of the Euler equations: reflection and interaction of oblique shock waves. The test consists of a cascade with an aspect ratio of 4% and $M_\infty = 1.40$. Plate 1 shows the final mesh and the Mach number distribution, and Plate 2 shows the pressure distribution. A comparison with finite difference solutions obtained with finer grids reveals that the same quality of solution is obtained using the DG approximation with significantly fewer elements.

The next test case is the simulation of inviscid flow around the shuttle orbiter at $M_\infty = 7.40$ and attack angle 40°. The objective of this simulation is to compare the pressure coefficient from wind tunnel experiments [33] and the values obtained using numerical simulation. The perfect gas model is used in the computations, since high-temperature effects were not present in the wind tunnel experiment.

Given that the geometry of the aft section of the vehicle has been simplified, the comparisons with wind tunnel data should be made only forward of the elevon hinge-line. This simplification is justified because the flow in the aft region is predominantly supersonic; consequently, the modeling of the geometry past the elevon hinge-line has negligible upstream influence.

The solution is obtained using mesh sequencing, starting with a grid of $25 \times 42 \times 37$ linear elements, executing the final iterations on a grid of $50 \times 84 \times 74$ linear elements.

Plate 3 shows the streamline pattern and Plate 4 the Mach number distribution at two normal planes. A comparison between the pressure coefficient from wind tunnel experiments [33] and the values obtained using numerical simulation is shown in Figure 4 for the centerline, and in Figure 5 for a cross-section station $z/L = 0.6$ (from nose to tail). The latter figure shows the pressure coefficient as a function of the angle around the body.

These numerical results indicate that the dominant inviscid flow features are well-predicted on the windward and leeside of the Shuttle Orbiter at a high angle of attack. As expected, the aft portion of the vehicle is not well-modeled past $z/L = 0.8$ due to the geometric simplifications introduced in the mesh past the elevon hinge-line.

Solutions to the incompressible Navier–Stokes equations are obtained using the artificial compressibility technique. The energy equation is not included, and the system is closed with a barotropic model $p = c^2(\rho - \rho_0)$, where c^2 is a positive constant chosen so that $c^2 \gg V^2_{\max}$ (velocity modulus squared), and ρ_0 is a reference density. The continuity equation

$$\frac{\partial \rho}{\partial t} + \beta \frac{\partial}{\partial x_i}(\rho u_i) = 0$$

includes the artificial compressibility parameter $\beta \in (0, 1]$. Using β, the inviscid pressure waves have the following velocities:

$$V \pm \sqrt{V^2 + \beta(c^2 - V^2)}, \qquad V^2 = \sum_{i=1}^{d} u_i^2.$$

The test cases selected are two widely used benchmarks for laminar viscous flows, the driven cavity problem at *Re* 3200 and 7500 as described in [34].

The solutions are obtained with a mesh of quadratic elements, which is equivalent (in number of degrees of freedom) to a mesh of 60×60 linear elements (used for plotting results) as shown in Plate 5, this figure also shows the pressure distribution on the background. Note that the pressure range shown is considerably narrower than the actual range, which is very wide because of the presence of singularities at the top corners of the cavity. The cut-off values

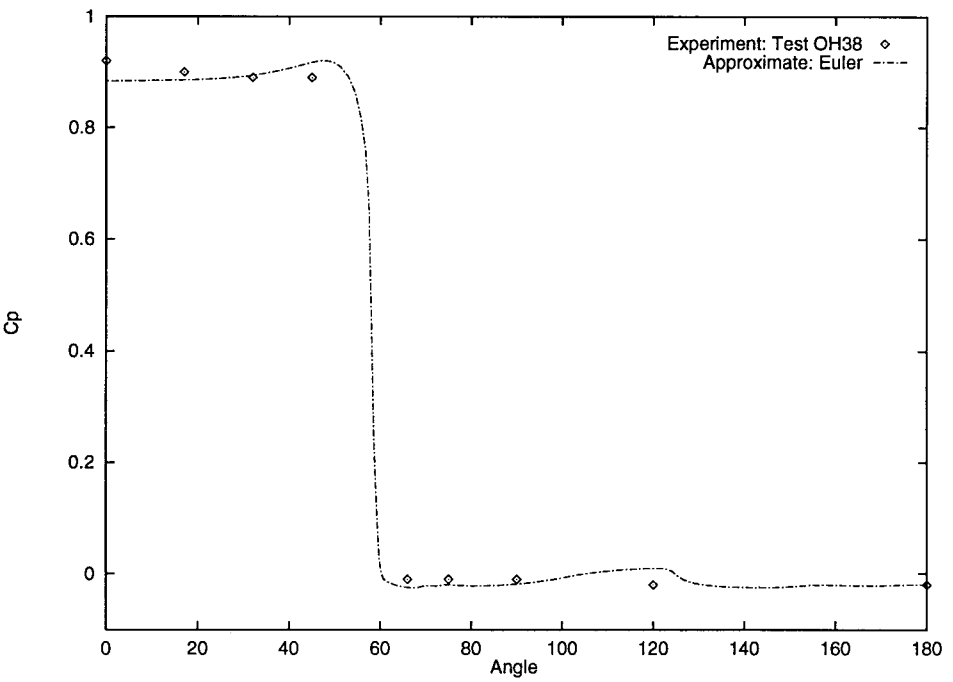

Figure 5. Pressure coefficient at the fuselage station $Z/L = 0.6$.

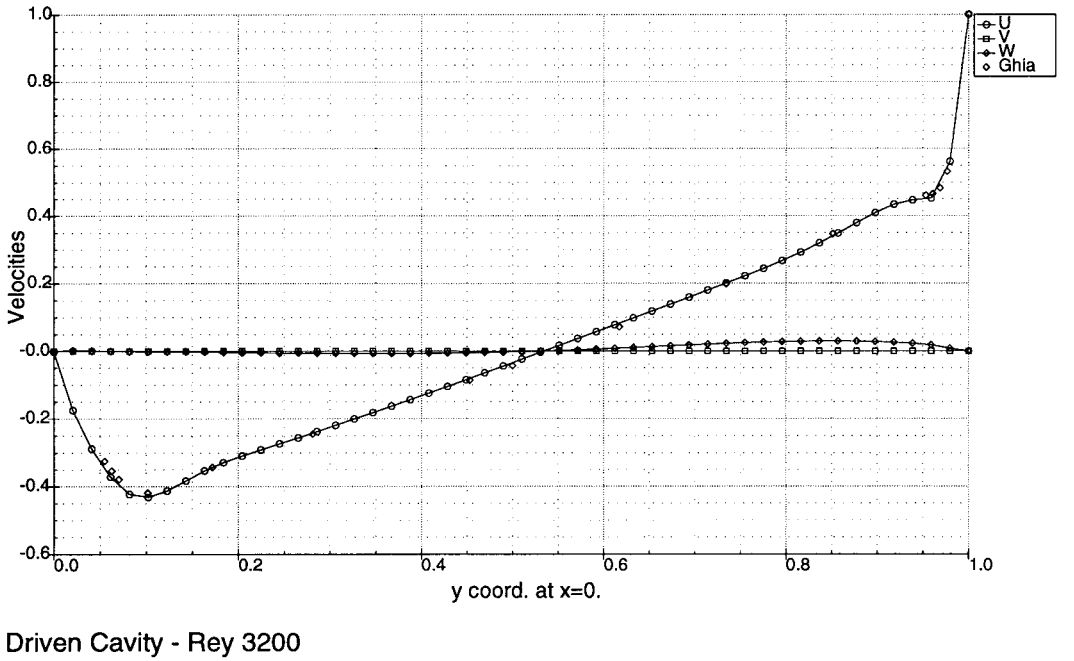

Figure 6. Comparison of horizontal velocity through the middle vertical plane.

$[p_{\min}, p_{\max}]$ applied to the range of pressure allow to observe small changes within the domain, excluding the areas adjacent to the top corners. Plate 6 shows the streamline pattern.

A comparison with high resolution values (*Re* 3200 case) reported in [34] for the horizontal velocity at the middle vertical plane is shown in Figure 6 and a comparison of vertical velocity at the middle horizontal plane is shown in Figure 7. These comparisons indicate that highly accurate velocity profiles can be obtained with a very coarse mesh using the present formulation.

8. CONCLUSIONS

A new discontinuous Galerkin technique for the solution of the Euler and Navier–Stokes equations is developed as an extension of the method presented in [8,9]. The formulation is compact with elementwise discontinuous basis functions, is locally or elementwise conservative, does not require auxiliary variables as mixed methods, and produces a mass matrix that is block diagonal (uncoupled blocks) for any degree of the polynomial basis functions. For diffusion-dominated problems, the order of the local polynomial approximations should be greater or equal to 2.

The structure of this discontinuous Galerkin method, particularly the fact that the degrees of freedom of an individual element are coupled only with those of neighbors sharing a boundary, suggest that the method is easily parallelizable. Parallel algorithms based on the method are the subject of future research.

A stability analysis and *a priori* error estimates are developed for the scalar case in [8,9], and numerical evidence presented in the previous section suggests that this formulation is highly reliable for obtaining numerical solutions to problems characterized by a wide range of fluid

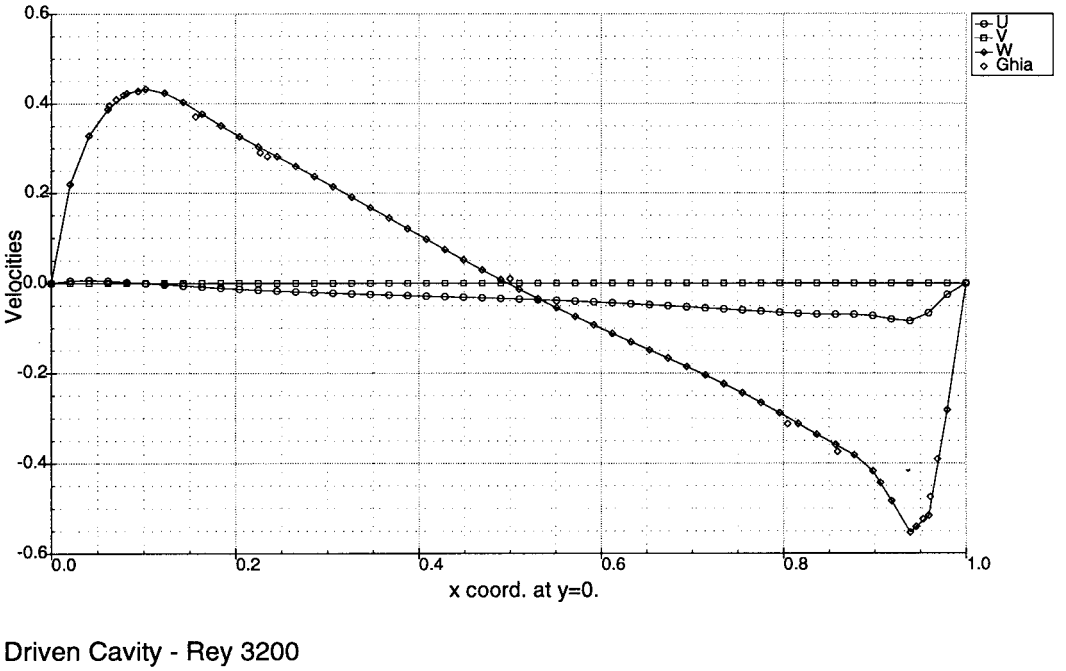

Figure 7. Comparison of vertical velocity through the middle horizontal plane.

flow conditions. Remarkably, this formulation is stable even when the flow field is not well-resolved, and does not produce the classical oscillations near sharp gradients (e.g. boundary layers), which are characteristic in classical H^1 approximations of underresolved boundary layers.

ACKNOWLEDGMENTS

The support of this work by the Army Research Office under grant DAAH04-96-0062 is gratefully acknowledged.

REFERENCES

1. A. Harten and S. Osher, 'Uniformly high-order accurate non-oscillatory schemes', *SIAM J. Numer. Anal.*, **24**, 279–309 (1987).
2. B. Van Leer, 'Towards the ultimate conservative difference scheme. III. Upstream-centered finite difference schemes for ideal compressible flow', *J. Comp. Phys.*, **23**, 263–175 (1977).
3. P.R. Woodward and P. Colella, 'The piecewise parabolic method (PPM) for gas dynamical calculations', *J. Comput. Phys.*, **54**, 174–201 (1984).
4. P.L. Roe, 'Error estimates for cell-vertex solutions of the compressible Euler equations', *Technical Report 87-6*, ICASE, January 1987.
5. E. Turkel, S. Yaniv and U. Landau, 'Accuracy of schemes for the Euler equations with non-uniform meshes', *Technical Report 85-59*, ICASE, December 1985.
6. I. Babuška, C.E. Baumann and J.T. Oden, 'A discontinuous *hp* finite element method for diffusion problems: 1D analysis', *TICAM Report 97-22*, also *Comput. Math. Appl.*, **37**, 103–122 (1999).
7. C.E. Baumann, 'A *hp*-adaptive discontinuous finite element method for computational fluid dynamics', *Ph.D. Dissertation*, The University of Texas at Austin, August 1997.
8. C.E. Baumann and J.T. Oden, 'A discontinuous *hp* finite element method for convection–diffusion problems', *Comput. Methods Appl. Mech. Eng.* (1998) to appear.

9. J.T. Oden, I. Babuška and C.E. Baumann, 'A discontinuous *hp* finite element method for diffusion problems', *TICAM Report 97-21*, also *J. Comput. Phys.*, **146**, 491–519 (1998).
10. L.M. Delves and C.A. Hall, 'An implicit matching principle for global element calculations', *J. Inst. Math. Appl.*, **23**, 223–234 (1979).
11. J. Nitsche, 'Über ein Variationsprinzip zur Lösung von Dirichlet Problemen bei Verwendung von Teilräumen, die keinen Randbedingungen unterworfen sind', *Abh. Math. Sem. Univ. Hamburg*, **36**, 9–15 (1971).
12. F. Bassi and R. Rebay, 'A high-order accurate discontinuous finite element method for the numerical solution of the compressible Navier–Stokes equations', *J. Comput. Phys.* (1997) submitted.
13. F. Bassi, R. Rebay, M. Savini and S. Pedinotti, 'The discontinuous Galerkin method applied to CFD problems', *2nd Europ. Conf. on Turbomachinery*, *Fluid Dynamics and Thermodynamics*, ASME, 1995.
14. I. Lomtev and G.E. Karniadakis, 'A discontinuous Galerkin method for the Navier–Stokes equations', *Int. J. Numer. Methods Fluids* (1997) submitted.
15. I. Lomtev and G.E. Karniadakis, 'Simulations of viscous supersonic flows on unstructured meshes', *AIAA-97-0754*, 1997.
16. I. Lomtev, C.B. Quillen and G.E. Karniadakis, 'Spectral/*hp* methods for viscous compressible flows on unstructured 2D meshes', *J. Comput. Phys.* (1998) to appear.
17. I. Lomtev, C.W. Quillen and G. Karniadakis, 'Spectral/*hp* methods for viscous compressible flows on unstructured 2D meshes', *Technical Report*, Center for Fluid Mechanics Turbulence and Computation, Brown University, Providence, RI 02912, 1996.
18. T.C. Warburton, I. Lomtev, R.M. Kirby and G.E. Karniadakis, 'A discontinuous Galerkin method for the Navier–Stokes equations on hybrid grids', Center for Fluid Mechanics 97-14, Division of Applied Mathematics, Brown University, 1997.
19. B. Cockburn and C.W. Shu, 'The local discontinuous Galerkin method for time dependent convection–diffusion systems', *SIAM J. Numer. Anal.* (1997) submitted.
20. P.G. Ciarlet, *The Finite Element Method for Elliptic Problems*, North-Holland, Amsterdam, 1978.
21. J.T. Oden and G.F. Carey, *Texas Finite Elements Series Vol. IV. Mathematical Aspects*, Prentice-Hall, Englewood Cliffs, NJ, 1983.
22. J.T. Oden and J.N. Reddy, *An Introduction to the Mathematical Theory of Finite Elements*, Wiley, New York, 1976.
23. K.S. Bey, 'An hp-Adaptive discontinuous Galerkin method for hyperbolic conservation laws', *Ph.D. Dissertation*, The University of Texas at Austin, May 1994.
24. B. Cockburn, S. Hou and C.W. Shu, 'TVB Runge–Kutta local projection discontinuous Galerkin finite element for conservation laws. IV. The multi-dimensional case', *Math. Comp.*, **54**, 545 (1990).
25. B. Cockburn, S. Hou and C.W. Shu, 'The Runge–Kutta discontinuous Galerkin method for conservation laws. V. Multi-dimensional systems', *ICASE Report 97-43*, 1997.
26. B. Cockburn, S.Y. Lin and C.W. Shu, 'TVB Runge–Kutta local projection discontinuous Galerkin finite element for conservation laws. III. One-dimensional systems', *J. Comput. Phys.*, **84**, 90–113 (1989).
27. B. Cockburn and C.W. Shu, 'TVB Runge–Kutta local projection discontinuous Galerkin finite element for conservation laws. II. General framework', *Math. Comput.*, **52**, 411–435 (1989).
28. C. Johnson and J. Pitkaranta, 'An analysis of the discontinuous Galerkin method for a scalar hyperbolic equation', *Math. Comput.*, **46**, 1–26 (1986).
29. P. Lesaint, 'Finite element methods for symmetric hyperbolic equations', *Numer. Math.*, 244–255 (1973).
30. P. Lesaint and P.A. Raviart, 'On a finite element method for solving the neutron transport equation', in C. de Boor (ed.), *Mathematical Aspects of Finite Elements in Partial Differential Equations*, Academic Press, New York, 1974, pp. 89–123.
31. P. Lesaint and P.A. Raviart, 'Finite element collocation methods for first-order systems', *Math. Comput.*, **33**, 891–918 (1979).
32. I. Babuška and M. Suri, 'The *hp*-version of the finite element method with quasi-uniform meshes', *Math. Model. Numer. Anal.*, **21**, 199–238 (1987).
33. W.H. Dye and T. Polek, 'Results of pressure distribution tests on a 0.010-scale space shuttle orbiter (61-0) in the Nasa/arc 3.5-foot hypersonic wind tunnel (test oh38)', *Technical Report*, NASA, 1975.
34. U. Ghia, K.N. Ghia and C.T. Shin, 'High-Re solutions for incompressible flow using the Navier–Stokes equations and a multigrid method', *J. Comput. Phys.*, **48**, 387–411 (1982).

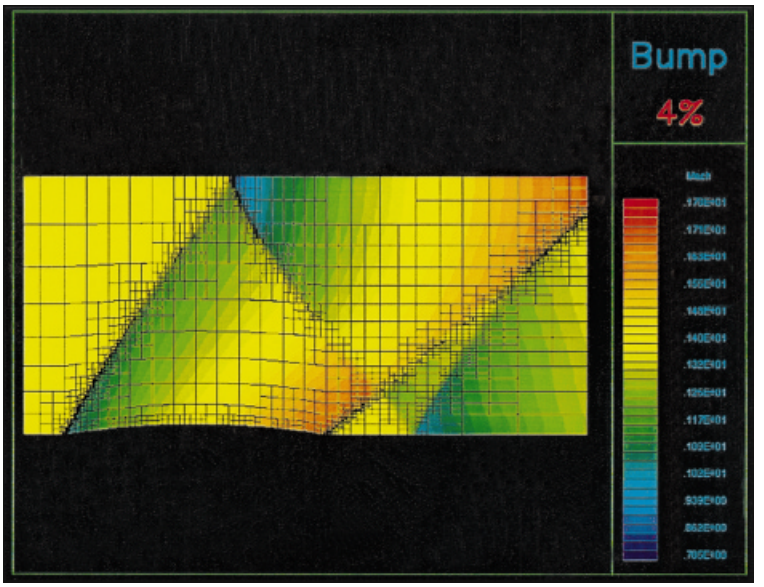

Plate 1. Cascade, aspect ratio 4%, $M_\infty = 1.40$, mesh and Mach number.

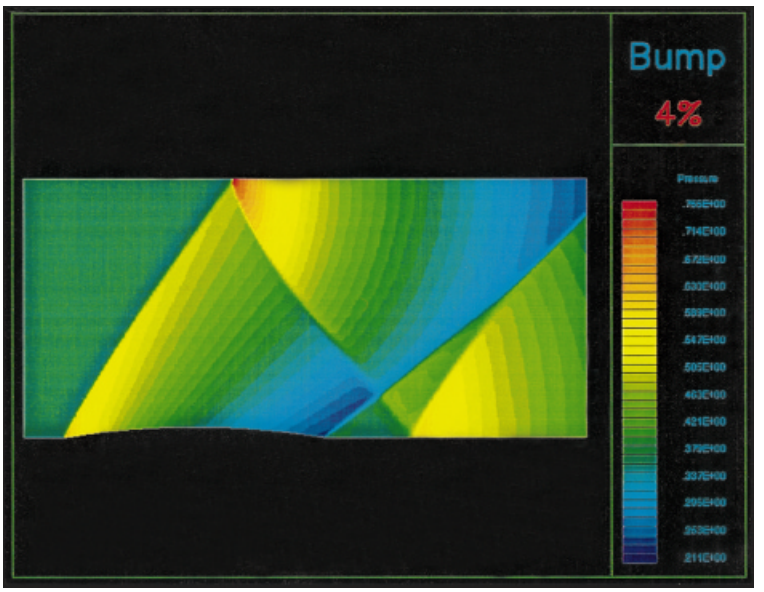

Plate 2. Cascade, aspect ratio 4%, $M_\infty = 1.40$, pressure.

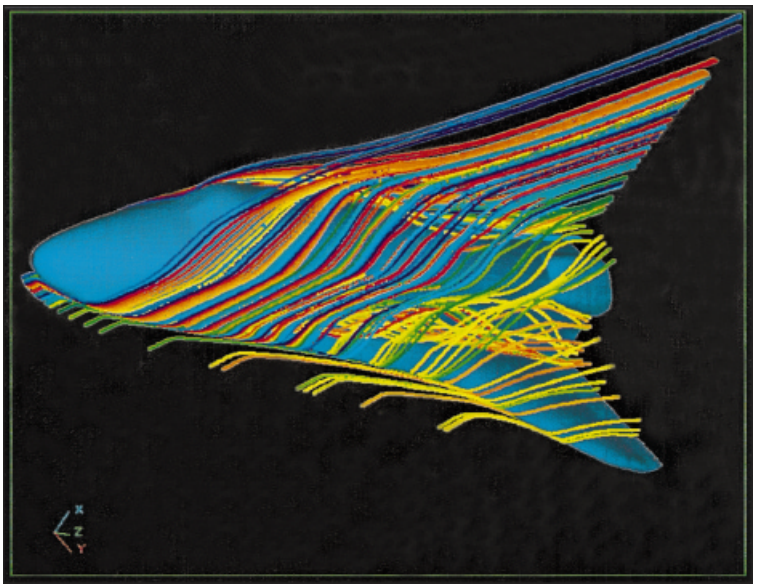

Plate 3. Shuttle Orbiter, $M_\infty = 7.4$, incidence 40.0°, streamlines.

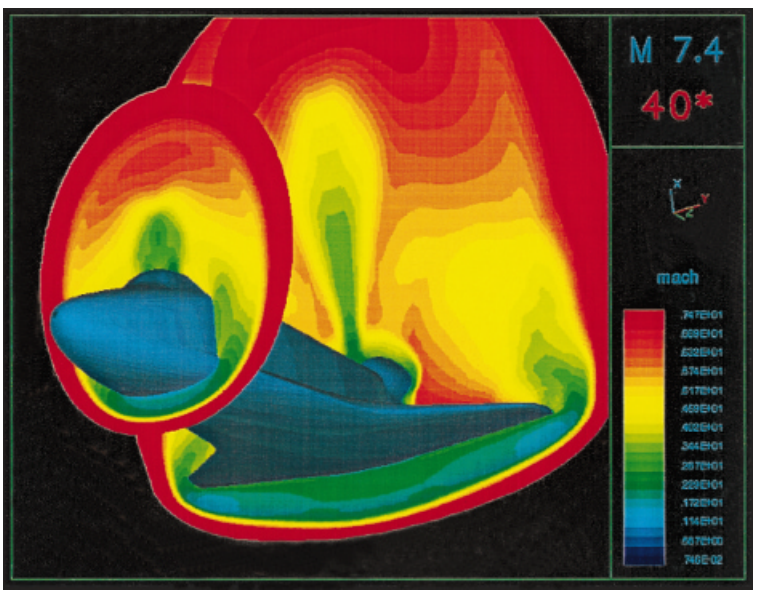

Plate 4. Shuttle Orbiter, $M_\infty = 7.4$, incidence 40.0°, Mach number.

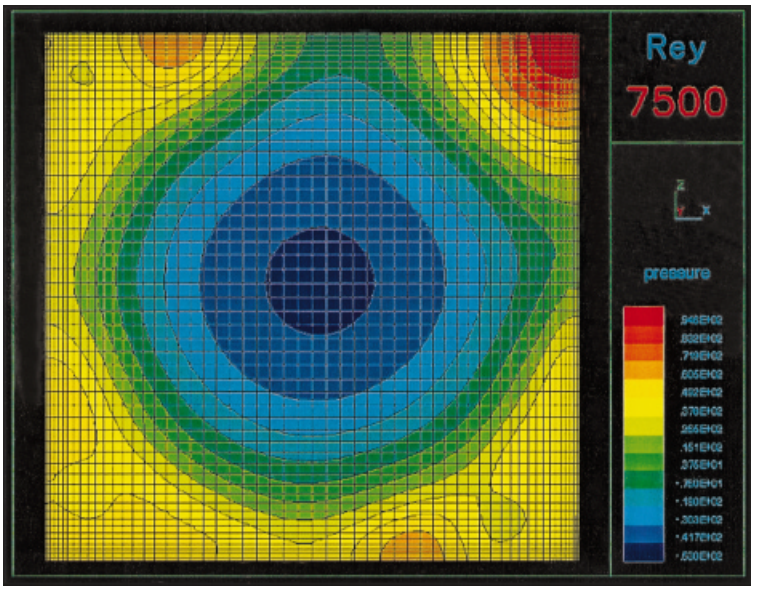

Plate 5. Driven cavity at $Re = 7500$: mesh and pressure contours.

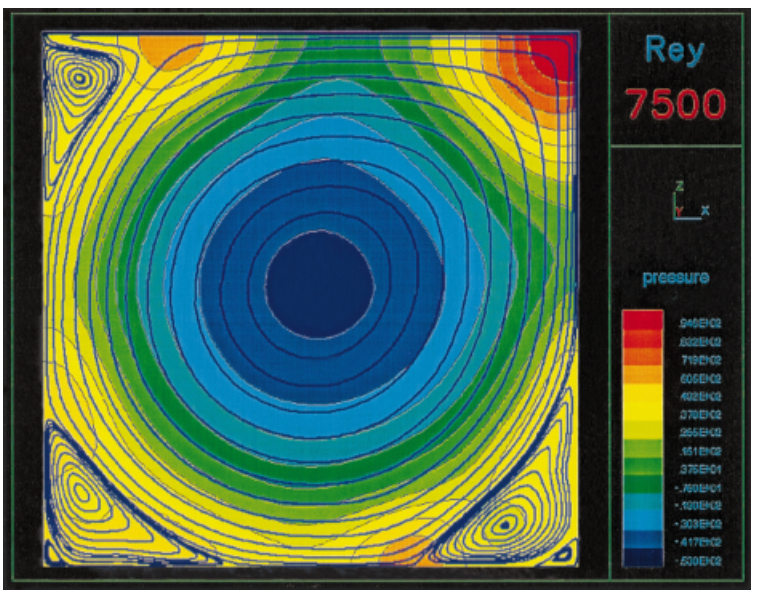

Plate 6. Driven cavity at $Re = 7500$: pressure contours and streamlines.